Simplified Wake Vortex Encounter Modeling and Inner Loop Controller Analysis for Small UAS

Justin J. Matt*, Zhenghao Lin †, and Haiyang Chao ‡
University of Kansas, Lawrence, KS 66045

Zhongquan Charlie Zheng §
Utah State University, Logan, UT 84322

Wake vortices generated by manned aircraft pose a significant hazard to the safe operation of UAS at and near airports. To analyze this hazard, a simplified methodology for modeling and simulating small UAS wake vortex encounters is proposed. The wake vortex is approximated as a spatially-linear varying wind field, which allows for seamless integration with standard flight dynamic models. This simplified approach is suitable for evaluation and categorization of the safety hazard introduced by wake vortex encounters for UAS operations, as it can be rapidly developed and applied to a variety of UAS and wake encounter scenarios. Additionally, since unmanned aircraft typically operate with some level of automatic control, roll and pitch hold controllers are designed to assess the impact of inner loop flight control design on the severity of the wake encounter. Simulation results showed that controllers designed for maximum disturbance rejection lead to noticeable attenuation of the UAS response to prolonged wake vortex encounters.

Nomenclature

DRB, DRP	=	disturbance rejection bandwidth and disturbance rejection peak
GM, PM	=	gain margin and phase margin
WVE	=	wake vortex encounter
C_L, C_y, C_D	=	lift, side-force, and drag coefficients
C_l, C_m, C_n	=	rolling, pitching, and yawing moment coefficients
K_p, K_i, K_d	=	proportional, integral, and derivative controller gains
L, M, N	=	rolling, pitching, and yawing moments
a_x, a_y, a_z	=	x-, y-, and z-axis body accelerations
b_0, r_c	=	wake vortex separation distance and core radius
f_x, f_y, f_z	=	x-, y-, and z-axis body forces
p_n, p_e, p_d	=	UAS North-East-Down position
p, q, r	=	roll, pitch, and yaw rates
p_g, q_g, r_g	=	x-, y-, and z-axis wake-induced rotational velocity components
p_r, q_r, r_r	=	air-relative roll, pitch, and yaw rates
u, v, w	=	x-, y-, and z-axis body velocities
u_g, v_g, w_g	=	body x-, y-, and z-axis wake-induced velocity components
u_r, v_r, w_r	=	x-, y-, and z-axis air-relative body velocities
Γ	=	wake vortex circulation
α, β	=	angle of attack and angle of sideslip
$\delta_e, \delta_a, \delta_r$	=	elevator, aileron, and rudder deflection
ζ, ω_n	=	damping coefficient and natural frequency
ϕ, θ, ψ	=	roll, pitch, and yaw angles

*M.S. Student, Department of Aerospace Engineering, University of Kansas, justinjmatt@gmail.com.
†Ph.D. Student, Department of Aerospace Engineering, University of Kansas.
‡Associate Professor, Department of Aerospace Engineering, University of Kansas, chaohaiyang@ku.edu.
§Professor and Head, Department of Mechanical and Aerospace Engineering, Utah State University.

I. Introduction

Unmanned aircraft systems (UAS) have been increasingly used in many industries to help improve operational efficiency and increase autonomy. At airports, for example, UAS could be used to assist with operations like facility inspection or weather forecasting. Additionally, next-generation unmanned aircraft, such as package-delivery UAS or urban air mobility (UAM) vehicles, will likely operate at airports together with manned aircraft in the future. To ensure safe integration of UAS into the controlled airspace, many factors must be considered, including the risk of wake vortex encounters (WVEs).

Wake vortices are one of the primary hazards for manned aircraft during takeoff and landing operations. In the past, substantial efforts have been devoted to determining safe separation distances between two aircraft departing from or approaching the same airport. As this problem involves many types of aircraft, simple methods are typically preferred for hazard determination and categorization efforts, such as the ICAO RECAT project [1, 2]. For manned aircraft, wake-induced rolling moment is the most commonly used metric for assessing the severity of WVEs during takeoff and landing. Several simplified analytical models have been developed to predict the wake-induced rolling moment [3, 4] and have been used in wake re-categorization efforts. Other methods, such as strip theory, vortex lattice methods, or high-order computational fluid dynamics-based approaches have also been used to simulate an aircraft's response to wake vortex encounters [5–8].

Currently, no such wake hazard model or categorization standards exist for small UAS. FAA wake separation regulations group together all aircraft with a maximum takeoff weight of 15,400 lbs or less [9]. To avoid hazards introduced by potential airspace sharing, UAS facility maps are used to limit UAS operating altitudes near airports. However, future UAS like package-delivery drones may operate at the same airport as manned aircraft. To ensure safe operation of these UAS at or near airports, new regulations are needed. These regulations should be supported by a combination of experimental and simulation analysis that includes a variety of UAS with different sizes, configurations, and weights.

UAS WVEs have been investigated less significantly than manned aircraft WVEs. In [10, 11], simulation studies were performed for urban air mobility vehicles subject to wake turbulence in urban environments. WVEs for small UAS in formation flight were simulated using a vortex lattice method and validated with flight data in [12, 13]. In [14], this capability was extended for another small UAS encountering the wake generated by a variety of manned aircraft. However, many of these methods required explicit geometry definition or use other computational techniques that are not suitable for rapid simulation of many different WVE scenarios.

In this paper, a simplified WVE modeling method is proposed for rapid simulation of UAS WVEs. This method can be adapted easily to different UAS and WVE scenarios. The proposed method approximates the wake vortex as a spatially-linear varying wind field, which allows for efficient computation of the forces and moments generated by the UAS using standard flight dynamic models. Explicit definition of exact UAS geometry is not required, as with many numerical methods. Additionally, the impact of the inner loop attitude controller during small UAS WVEs is evaluated using the proposed modeling method. Two controllers are designed using slightly different specifications to quantify the effect of different control specifications on the UAS WVE response.

This paper is organized as follows. In Section II, the problem is described. Then, in Section III, the wake vortex encounter modeling methodology is presented. The controller design procedure is discussed in SectionIV, and simulation results are presented in Section V. Lastly, conclusions and recommendations for future research directions are provided in Section VI.

II. Problem Description

Different wake vortex encounter scenarios may result in different hazards to UAS safety. This is illustrated in Fig. 1. For example, if a UAS is crossing perpendicularly to a larger aircraft's flight path, it may result in stall, large pitch excursions, or large vertical loads. These hazards can cause loss of control or structural failure of the UAS. In contrast, a small UAS may experience large rolling moments if it follows the path of the wake-generating aircraft and may fly into the vortex core. Lastly, flight through the midpoint of a vortex pair may result in rapid altitude loss caused by the large down-draft created by the vortices. This could cause the UAS to crash during low altitude operations such as takeoff and landing.

Methods to predict the UAS response are needed to evaluate the hazard of these different WVE scenarios. The response can be quantified by flight measurements such as altitude loss, airflow angle changes, attitude angle and rate changes, or body acceleration spikes.

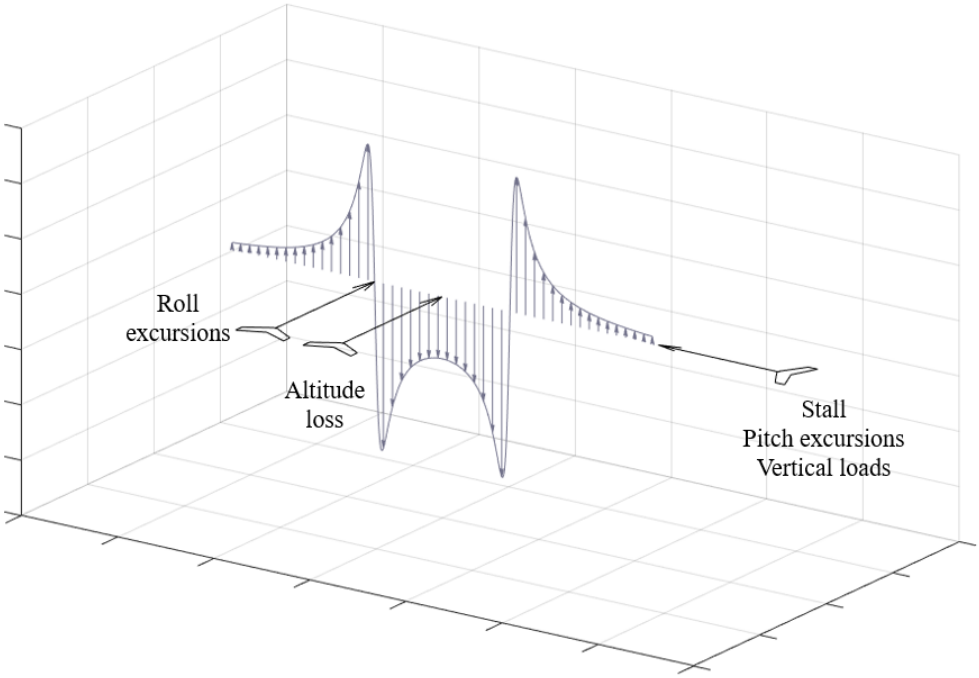

Fig. 1 Small UAS wake vortex encounter.

Numerical methods are often used to compute the aerodynamic response of an aircraft to a WVE, including strip theory methods [5, 7, 8], vortex lattice methods [6, 14], or other high-order CFD-based methods. However, to identify the hazards for a wide variety of UAS and WVE scenarios, it is desired to use a simplified methodology that can be quickly applied to many small UAS. Ideally, limited information about the UAS should be needed for simulation. If these requirements are met, a large-scale simulation and experiment campaign effort can be performed to characterize and categorize the hazards faced by small UAS during WVEs, similar to what has been done in the past for manned aircraft. The goal of this paper is to develop a simplified UAS WVE modeling methodology that allows for rapid simulation using standard flight dynamics models. This methodology is demonstrated on a representative small UAS, discussed in the next section, and the influence of the inner loop flight controller on the encounter severity is evaluated.

A. UAS Dynamic Models

Flight dynamics model often consist of twelve ordinary differential equations (ODEs) that describe the rigid-body translational and rotational kinematics and dynamics. In state space form these equations can be written as follows [15].

Translational kinematics

$$\begin{bmatrix} \dot{p}_n \\ \dot{p}_e \\ \dot{p}_d \end{bmatrix} = \begin{bmatrix} \mathrm{c}_\theta \mathrm{c}_\psi & \mathrm{s}_\phi \mathrm{s}_\theta \mathrm{c}_\psi - \mathrm{c}_\phi \mathrm{s}_\psi & \mathrm{c}_\phi \mathrm{s}_\theta \mathrm{c}_\psi + \mathrm{s}_\phi \mathrm{s}_\psi \\ \mathrm{c}_\theta \mathrm{s}_\psi & \mathrm{s}_\phi \mathrm{s}_\theta \mathrm{s}_\psi + \mathrm{c}_\phi \mathrm{c}_\psi & \mathrm{c}_\phi \mathrm{s}_\theta \mathrm{s}_\psi - \mathrm{s}_\phi \mathrm{c}_\psi \\ -\mathrm{s}_\theta & \mathrm{s}_\phi \mathrm{c}_\theta & \mathrm{c}_\phi \mathrm{c}_\theta \end{bmatrix} \begin{bmatrix} u \\ v \\ w \end{bmatrix} \tag{1}$$

Translational dynamics

$$\begin{bmatrix} \dot{u} \\ \dot{v} \\ \dot{w} \end{bmatrix} = \begin{bmatrix} rv - qw \\ pw - ru \\ qu - pv \end{bmatrix} + \frac{1}{m} \begin{bmatrix} f_x \\ f_y \\ f_z \end{bmatrix} \tag{2}$$

Rotational kinematics

$$\begin{bmatrix} \dot{\phi} \\ \dot{\theta} \\ \dot{\psi} \end{bmatrix} = \begin{bmatrix} 1 & \sin\phi \tan\theta & \cos\phi \tan\theta \\ 0 & \cos\phi & -\sin\phi \\ 0 & \frac{\sin\phi}{\cos\theta} & \frac{\cos\phi}{\cos\theta} \end{bmatrix} \begin{bmatrix} p \\ q \\ r \end{bmatrix} \tag{3}$$

Rotational dynamics

$$\begin{bmatrix} \dot{p} \\ \dot{q} \\ \dot{r} \end{bmatrix} = \begin{bmatrix} \Gamma_1 pq - \Gamma_2 qr \\ \Gamma_5 pr - \Gamma_6 (p^2 - r^2) \\ \Gamma_7 pq - \Gamma_1 qr \end{bmatrix} + \begin{bmatrix} \Gamma_3 L + \Gamma_4 N \\ M/I_{yy} \\ \Gamma_4 L + \Gamma_8 N \end{bmatrix} \tag{4}$$

where (p_n, p_e, p_d) are the North-East-Down (NED) position, (u, v, w) are the body x-, y-, and z-axis velocities, (ϕ, θ, ψ) are the roll, pitch, and yaw angles, (p, q, r) are the roll, pitch, and yaw rates, m is the UAS mass, I_{yy} is the y-axis moment of inertia, and $\Gamma_{i=1:8}$ are defined by the x- and z-axis moments and products of inertia, (I_{xx}, I_{zz}, I_{xz}) [15].

The body x-, y-, and z-axis forces, (f_x, f_y, f_z) and rolling, pitching, and yawing moments (L, M, N) are functions of aerodynamic, propulsive, and/or gravitational effects. Aerodynamic forces and moments are typically expressed as nondimensional coefficients that are functions of the aircraft state.

$$\begin{aligned} C_x(\alpha, q, \delta_e, ...) &= \frac{f_{x_{\text{aero}}}}{0.5\rho V^2 S} \\ C_y(\beta, p, r, \delta_a, \delta_r, ...) &= \frac{f_{y_{\text{aero}}}}{0.5\rho V^2 S} \\ C_z(\alpha, q, \delta_e, ...) &= \frac{f_{z_{\text{aero}}}}{0.5\rho V^2 S} \end{aligned} \tag{5}$$

$$\begin{aligned} C_l(\beta, p, r, \delta_a, \delta_r, ...) &= \frac{L}{0.5\rho V^2 S b} \\ C_m(\alpha, q, \delta_e, ...) &= \frac{M}{0.5\rho V^2 S c} \\ C_n(\beta, p, r, \delta_a, \delta_r, ...) &= \frac{N}{0.5\rho V^2 S b} \end{aligned} \tag{6}$$

where ρ is atmospheric density, V is the UAS airspeed, S is the UAS reference area, and b and c are the wingspan and chord length.

The equations above are just one example of a dynamic model structure that can be used. The proposed WVE simulation methodology is adaptable to different structures because the effect of the wake vortex is computed simply as changes to air-relative translational and rotational velocities. For example, linear dynamic models can also be used.

The KHawk-55 UAS is simulated to demonstrate the methods developed in this paper. The KHawk-55, pictured in Fig. 2, is a flying-wing UAS developed at the Cooperative Unmanned Systems Laboratory (CUSL) at the University of Kansas. The UAS has elevon control surfaces and a single electric brushless motor, a wingspan of 55 inches, a gross takeoff weight of 5.75 lbs, and the cruise airspeed is 18 m/s. Dynamic models were identified from flight data using frequency domain methods [16, 17].

Fig. 2 CUSL KHawk-55 UAS.

III. Methodology

In this section, the Linear Wind Field Approximation (LWFA) method is introduced to model the UAS response during wake vortex encounters. The overall structure is shown in Fig. 3. This method simulates small UAS wake vortex encounters by assuming the wake vortex surrounding the UAS is linearly varying along the UAS geometry [18]. The proposed method is implemented as a MATLAB/Simulink-based software, called HawkWakeSim v2.1-LWFA. Sample results comparing the proposed method with vortex lattice methods are provided for initial validation of this approach.

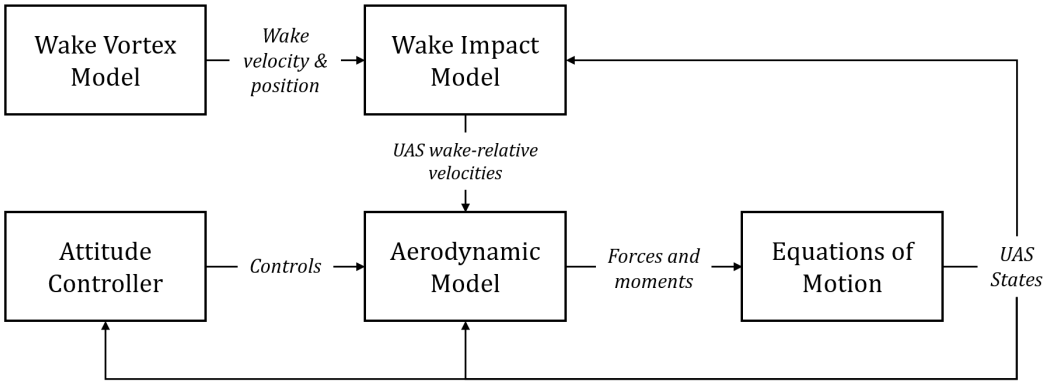

Fig. 3 System diagram for wake encounter modeling using the LWFA method.

A. Wake Vortex Encounter Models

The wake vortex encounter model consists of two main components. A wake vortex model is used to describe the flow field created by a lift generating aircraft. Then, a wake impact model is used to compute the effects of the wake vortices on the UAS encountering the wake. These components are combined with a flight dynamics model to create a six degree-of-freedom wake vortex encounter simulator.

1. Wake Vortex Model

The velocity field of the wake vortex is generated using the Burnham-Hallock model [19, 20]. This model was derived empirically from field measurements of commercial aircraft and has been commonly used for WVE simulation. The Burnham-Hallock model describes the tangential velocity of the vortex as a function of the radial distance, r.

$$v_\theta(r) = \frac{\Gamma}{2\pi r}\frac{r^2}{r_c^2 + r^2}, \tag{7}$$

where Γ is the vortex circulation and r_c is the core radius of the vortex. The core radius can be expressed as about 5.2% of the initial vortex spacing, b_0:

$$r_c = 0.052 b_0, \tag{8}$$

where

$$b_0 = \frac{\pi}{4} b \tag{9}$$

The vortex circulation is a function of the generating aircraft's weight, velocity, and wingspan. The circulation decays over time. The initial circulation can be computed as:

$$\Gamma_0 = \frac{mg}{\rho b_0 V} \tag{10}$$

where m is mass, g is acceleration due gravity, ρ is atmospheric density, and V is velocity.

In our simulations, the circulation strength is held constant since the WVE occurs over a short time interval. However, decay models such as the Sarpkaya model [21] can be combined with Eq. (10) to predict the wake circulation over time, given the generating aircraft's characteristics.

2. Wake Impact Model

Many methods have been used in the past to model the response of an aircraft to a wake vortex. Strip theory is one of the most popular methods and has been successfully validated with flight test data [8]. However, one disadvantage of strip theory is that the exact geometry of the aircraft is required for modeling. Other numerical methods face a similar challenge, since the exact UAS geometry may be unknown. Additionally, these methods usually require long development or computation times, which motivates the development of simplified models that are suitable for rapid simulation of different UAS and WVE scenarios.

A simplified method based on the linear wind field approximation [18] is used to model the effect of the wake vortex on the UAS response. The main benefit of this approach is in its simplicity; the only prior information required is a standard flight dynamics model and basic UAS characteristics such as wingspan and length. As such, it is suitable for performing rapid simulation of a wide range of UAS and WVE scenarios. A similar method was implemented in [22] to model the influence of wake vortices during aerial refueling operations and validated with wind tunnel data.

In this method, the wake vortex surrounding the UAS is approximated as a spatially-linear varying wind field using a first-order Taylor series expanded at the UAS center of gravity. Variations with respect to the body z-axis are assumed to be negligible.

$$\begin{aligned} u_g(x,y,t) &= u_{g_0}(t) + \frac{\partial u_g(t)}{\partial x}x + \frac{\partial u_g(t)}{\partial y}y, \\ v_g(x,y,t) &= v_{g_0}(t) + \frac{\partial v_g(t)}{\partial x}x + \frac{\partial v_g(t)}{\partial y}y, \\ w_g(x,y,t) &= w_{g_0}(t) + \frac{\partial w_g(t)}{\partial x}x + \frac{\partial w_g(t)}{\partial y}y, \end{aligned} \tag{11}$$

The gradients $\partial u_g/\partial x$ and $\partial v_g/\partial y$ represent strains in velocity fields that can also be assumed to be negligible [18].

Linear gradients of downwash are equivalent to induced rotational velocities. Thus, we write the downwash derivatives as

$$p_g = \frac{\partial w_g}{\partial y}, \tag{12}$$

$$q_g = -\frac{\partial w_g}{\partial x}, \tag{13}$$

Similarly, a nonzero yaw rate will create induced tangential velocities at different points on the UAS. However, depending on the point on the aircraft, the tangential velocity may be in the x-direction, y-direction, or both. As such, the last two gradients both cause similar effects as yaw rate, and are denoted

$$r_g = \frac{\partial v_g}{\partial x} - \frac{\partial u_g}{\partial y} \tag{14}$$

The forces and moments generated by the UAS are a function of the UAS's velocity relative to the surrounding air. As such, we express the UAS velocities relative to the air, denoted by a subscript r, as the difference between the inertial velocities and wake-induced velocities, denoted by a subscript g, which come from the terms of the Taylor series expansion.

$$\begin{aligned} u_r &= u - u_{g_0}, & p_r &= p - p_g, \\ v_r &= v - v_{g_0}, & q_r &= q - q_g, \\ w_r &= w - w_{g_0}, & r_r &= r - r_g, \end{aligned} \tag{15}$$

The relative velocities are used with the respective aerodynamic model to compute the forces and moments generated by the UAS. Note that the inertial velocities are still used for kinematics and dynamics (Eqs. (1-4)).

The LWFA method can be implemented by generating a set of discrete points along the wing and fuselage of the UAS and computing the wake-induced velocity at each point using the Burnham-Hallock model. Then, the unknown terms of Eqs. (11) can be estimated using ordinary least squares regression. Though this requires certain knowledge of aircraft geometry, only rudimentary characteristics such as wingspan or total length are needed. Additionally, the method is relatively robust to different realizations of the discrete points. This is because only the average wind over the body of the aircraft needs to be estimated. In contrast, strip theory methods compute the exact forces and moments at each discrete point. The discrete points generated for the KHawk 55 UAS are shown in Fig. 4(a). An example of the approximated upwash field for points generated along two lines representing the wing and fuselage is also shown in Fig. 4(b).

B. Implementation and Comparison with Vortex Lattice Method

The proposed LWFA method is implemented in MATLAB/Simulink as one function of HawkWakSim v2.1. The vortex lattice method (VLM) for simulating wake vortex encounters from our previous research [14] was used to provide some cross validation of the proposed LWFA method. Static wake-induced aerodynamic coefficients at different lateral distances from the wake vortex core were calculated with both methods and compared. The KHawk-55 was used for simulation. The UAS was simulated at steady state conditions (wings-level at cruise speed) with the heading angle aligned with the wake-generating aircraft. The lateral spacing from the vortex core was varied, while the vertical spacing was held constant, in-line with the vortex core. The wake vortex has a circulation strength of 20 m^2/s and core radius of 0.45 m, representative of a Cessna-172. Fig. 5 shows the wake-induced force and moment coefficients calculated using the VLM and LWFA methods. The lift, rolling moment, and yawing moment prediction matches well between the two methods. However, the linear method predicts a larger pitching moment for the KHawk55. This provides some empirical validation of the LWFA approach, particularly for predicting wake-induced rolling moment and vertical loads, which are two main hazards faced during WVEs.

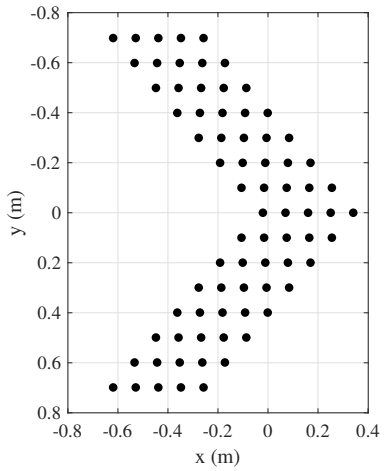

(a) Discrete points of KHawk55 UAS.

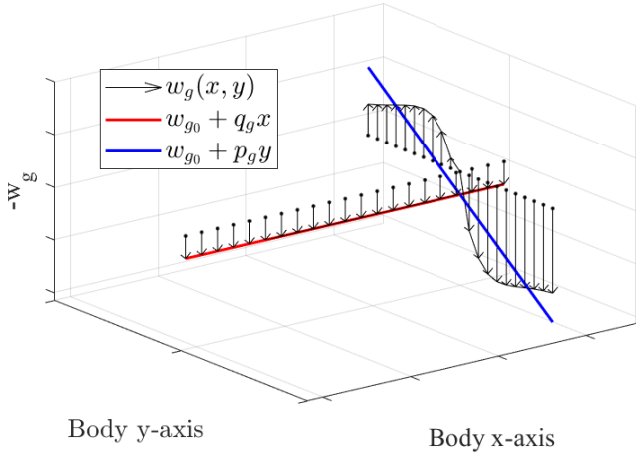

(b) Example of of approximated linear wind fields.

Fig. 4 Examples of LWFA method.

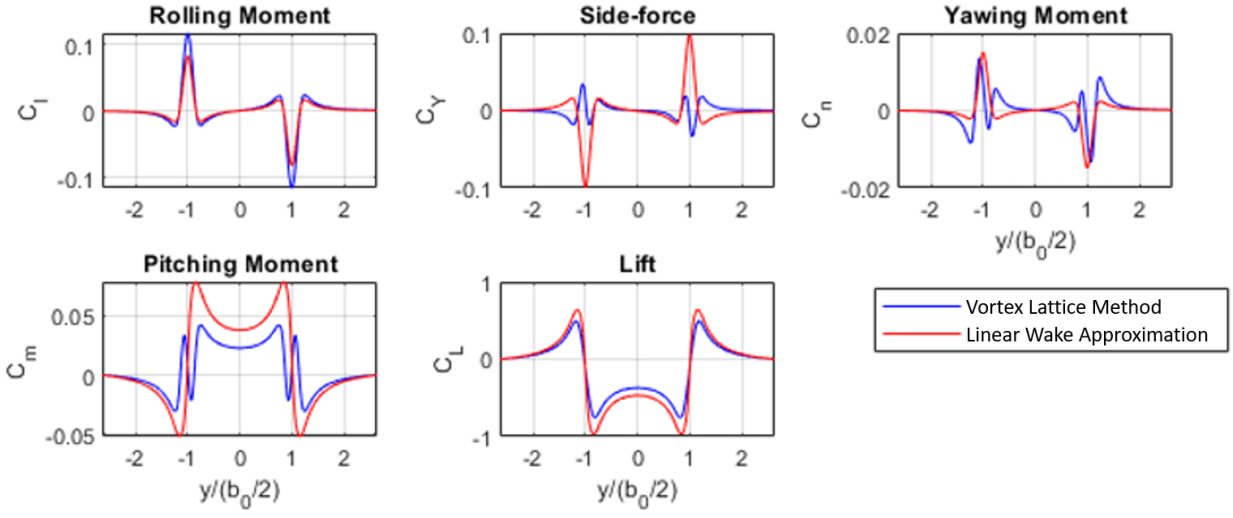

Fig. 5 Comparison between VLM and linear approximation for KHawk55 parallel wake encounter [14].

IV. Controller Design for Wake Disturbance Rejection

Most commercial UAS operate with some level of automatic control, such as inner loop attitude controllers or high-level path following control laws. As such, a unique aspect of the WVE problem for small UAS is characterizing the impact of the flight controller on the response to WVEs. In this section, the control design process is outlined. Initial controller specifications were selected to represent a nominal use-case. Then, specifications were relaxed, and a second controller was designed to maximize disturbance rejection. The objective of this process is to assess the relation between certain controller specifications and the wake disturbance rejection capability of the controller.

A. Control Law Structure

For the WVE problem, the low-level attitude control law will have the most significant impact on the UAS response, as the response is likely independent of most high-level guidance logic. As such, inner loop roll and pitch hold controllers were focused on in this paper.

A classical PID structure is used for both controllers, using attitude angle and rate feedback. PID controllers are very common for small UAS and have been shown to be effective for a wide range of UAS size and configurations, as evidenced by their wide use in open-source UAS autopilots, such as ArduPilot*, PX4†, and Paparazzi‡. Furthermore, the flexibility of PID controllers ensures the same control structure can be used for future simulations with different UAS, which is useful for later comprehensive analysis and comparisons. The control structure is shown in Fig. 6.

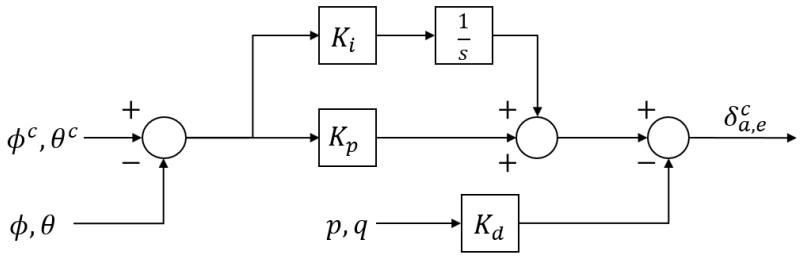

Fig. 6 Roll and pitch hold controller structure.

The controller computes commanded deflection angles that are sent to the servos, or actuators. The actuators are modeled by a second-order transfer function, which was identified from experimental data:

$$G_{\text{act}} = \frac{\omega_n^2}{s^2 + 2\zeta\omega_n s + \omega_n^2} \tag{16}$$

where $\omega_n = 30.7$ rad/s and $\zeta = 0.62$ are the natural frequency and damping coefficient of the actuator.

B. Controller Specifications

As no handling-quality or flight control system requirements exist for small UAS, selecting controller specifications can be a delicate task. For our application, it is important to select a set of specifications that is independent of UAS-specific parameters, such as size, weight, or configuration. Instead, we desire to select a set of specifications that can be used to design controllers for a variety of UAS. This provides a baseline for direct comparison of different UAS' response to the same wake vortex.

The specifications were selected based on manned aircraft handling quality and flight control system specifications [23–25] and existing literature for small UAS multi-objective control design [16, 26]. Two sets of specifications were used to design a nominal controller and a disturbance rejection controller.

*ArduPilot, https://ardupilot.org/ [Retrieved May 2022]

†PX4 Autopilot, https://px4.io/ [Retrieved May 2022]

‡Paparazzi UAV, https://wiki.paparazziuav.org [Retrieved May 2022]

1. Nominal Control Specifications

The first requirements deal with the stability of the single-input, single-output closed-loop systems, ϕ/ϕ^c and θ/θ^c. First, the system is required to be stable (all eigenvalues in the left-hand plane). Second, the stability margins of the loop gain broken at the actuator must meet the requirements:

$$\begin{aligned} &\text{Gain margin (GM)} > 6 \text{ dB} \\ &\text{Phase margin (PM)} > 45 \text{ deg} \end{aligned} \tag{17}$$

The next requirements deal with the damping of the closed-loop system. These requirements differ for the longitudinal and the lateral-directional dynamic modes. The damping is required to be above specified values depending on frequency:

$$\zeta_{\text{lon}} \geq \begin{cases} 0.04 & \omega_n < 1 \text{ rad/s} \\ 0.4 & 1 \leq \omega_n < 20 \text{ rad/s} \\ 0.25 & \omega_n \geq 20 \text{ rad/s} \end{cases} \tag{18}$$

$$\zeta_{\text{lat-dir}} \geq \begin{cases} 0.4 & \omega_n \leq 15 \text{ rad/s} \\ 0.3 & \omega_n > 15 \text{ rad/s} \end{cases} \tag{19}$$

The step response of the closed-loop system is required to have an overshoot less than 10%, and the gains are constrained based on the empirical methods discussed in [27].

$$\begin{aligned} K_i &\leq 0.4 K_p \\ K_d &\leq 0.15 K_p \end{aligned} \tag{20}$$

Lastly, minimum requirements for the disturbance rejection bandwidth (DRB) and disturbance rejection peak (DRP) are set. These criteria are defined based on the output sensitivity function of the roll or pitch angle, respectively. The DRB is computed as the frequency at which the sensitivity function crosses -3 dB, and the DRP is defined as the maximum magnitude of the sensitivity function. It has been shown that increasing DRB can lead to increased rejection of disturbances to the roll or pitch angles [28]. However, increasing DRB will also come at the cost of increasing DRP. The disturbance rejection requirements are

$$\begin{aligned} &\text{DRB} \geq 0.9 \text{ rad/s} \\ &\text{DRP} \leq 5 \text{ dB} \end{aligned} \tag{21}$$

The nominal controller was tuned by hand to achieve a desirable step response such that all specifications were met. A conservative design was selected to reduce the control surface activity.

2. Disturbance Rejection Controller

Several requirements were relaxed for the disturbance rejection controller, with the ultimate goal of increasing the DRB of the system. The stability margin and disturbance rejection specifications were relaxed by 20%. The minimum damping specification was reduced by 0.05 for all frequencies except the low-frequency longitudinal modes.

Additionally, the disturbance rejection controller was designed using an optimization strategy, rather than being tuned by hand. The DRB was maximized, subject to the constraints of the relaxed controller specifications. This was achieved by first performing a scatter analysis to identify a small search space. Then, pattern search optimization was performed to find the gain set that maximized the DRB. An example of this process is visualized in Fig. 7.

The roll and pitch controllers designed for the KHawk55 UAS are summarized in Table 1. The rise time is defined as the time required for the step response to change from 10% to 90% of the commanded value. The roll and pitch step responses with the two controllers are shown in Fig. 8. The increased gains of the disturbance rejection controller result in a faster but less damped response and higher control activity.

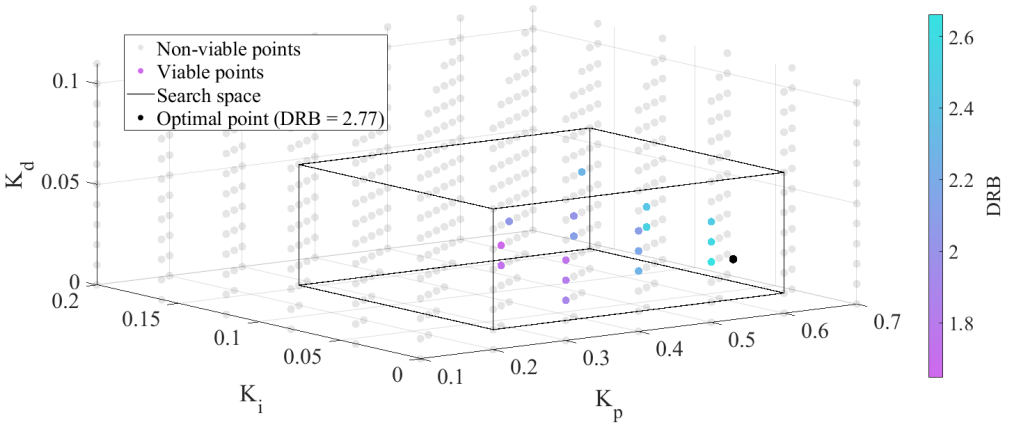

Fig. 7 Design of disturbance rejection controllers through optimization.

Table 1 KHawk55 roll and pitch controller specifications.

	Roll controller		Pitch controller	
Metric	**Nominal**	**Dist. Rej.**	**Nominal**	**Dist. Rej.**
K_p	0.3	0.530	0.20	0.383
K_i	0.02	0	0	0
K_d	0.029	0.030	0.015	0.011
Overshoot (%)	5.1	10.0	0	0
Rise Time (s)	0.75	0.21	0.88	0.13
GM (dB)	15.4	11.7	9.4	6.3
PM (deg)	76.2	44.3	101	87.0
DRB (rad/s)	1.8	2.8	2.3	4.9
DRP (dB)	3.0	5.5	2.5	6.0

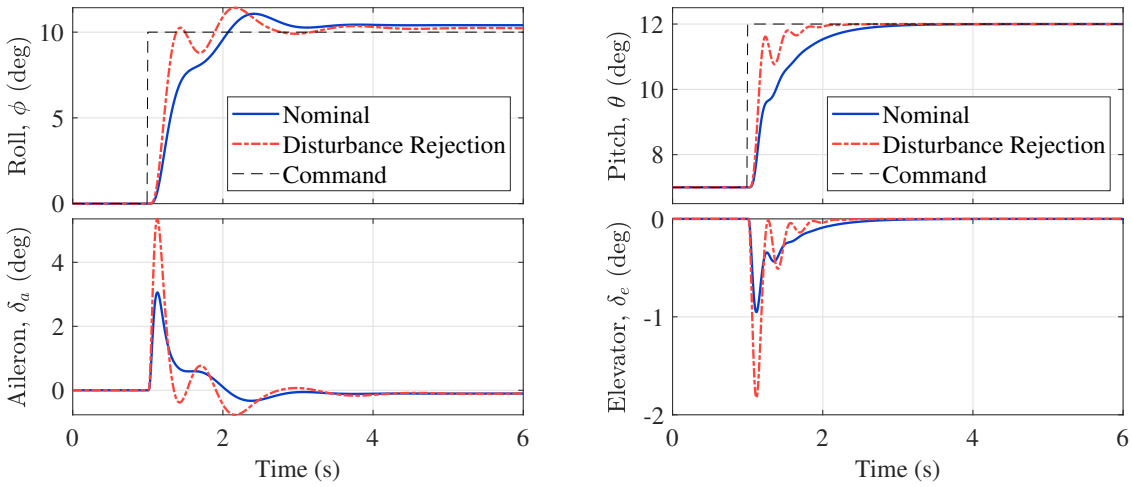

(a) Roll angle step response.

(b) Pitch angle step response.

Fig. 8 Closed-loop system step responses.

V. Simulation Results

The methods discussed previously can be used for rapid small UAS WVE simulation and controller performance evaluation. In this section, initial simulation results will be shown and discussed. Four WVE scenarios are presented to demonstrate the effects of wake encounter angle, core radius size, and circulation strength on the encounter severity and controller performance. The horizontal UAS flight trajectories for these four scenarios include 15, 30, and 90 deg encounter angles and are shown in Fig. 9. Note that the wake vortex core radii are represented by the width of the double lines in the figures. Response measurements such as roll and pitch angles, angular rates, body accelerations, and control activity are analyzed to evaluate severity and controller performance.

The first case analyzed is shown in Fig. 10. In Case 1, the UAS was simulated to encounter a wake vortex at a 30-degree angle. The wake was generated by an aircraft with a 30 m wingspan and has a circulation of 100 m^2/s and core radius of 1.2 m. This size of vortex is representative of a narrow-body airliner, such as a Boeing 737-800, that is about five miles away from the UAS.

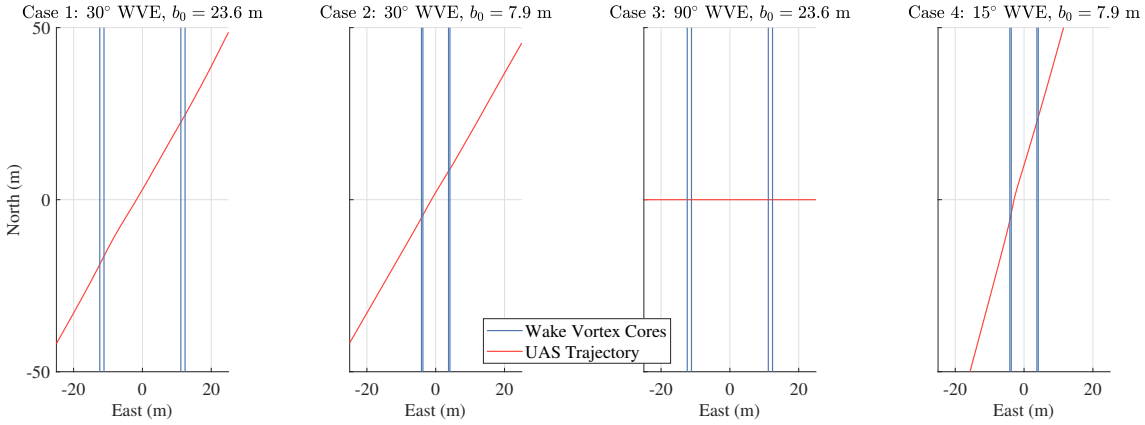

Fig. 9 KHawk-55 wake vortex encounter flight trajectories.

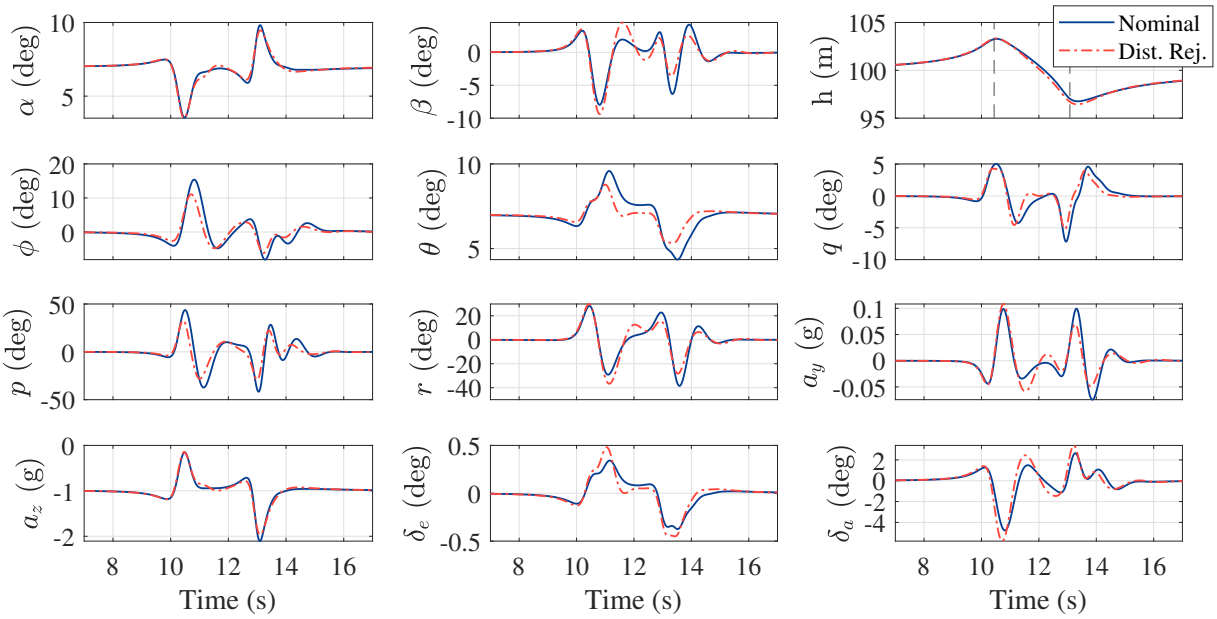

Fig. 10 Case 1: KHawk-55 30° wake vortex encounter (Γ = 100 m^2/s, b = 30 m, r_c = 1.2 m).

The primary response of the UAS can be observed in the roll angle and roll rate plots, where the disturbance rejection controller reduces the peak of each response by about 25%. The pitch angle response is also reduced. The controller successfully attenuates disturbances at the cost of more aggressive control commands, which can be seen in the aileron and elevator plots. Finally, the altitude plot shows the trajectory of the UAS, with the position of the wake cores shown as black, dashed lines. The wake vortex pushes the UAS above the first core, then causes the UAS to rapidly lose altitude and cross the second vortex several meters below the core.

The disturbance rejection controller was very effective under the conditions of the previous case. However, for rapid WVEs, characterized by small vortex radii or near-perpendicular encounter angles, the different controllers resulted in very little difference in the UAS response. This can be seen in the encounter shown in Fig. 11. The vortex was generated by an aircraft with a 10 m wingspan, has circulation strength of 20 m^2/s, and core radius of 0.4 m. This is representative of the wake of a single-engine general aviation aircraft. The controller cannot respond quickly enough and, as such, has less impact on the UAS response during the encounter. The UAS encounters both cores directly, rather than being pushed above and below the cores like in Case 1. Because of this, the UAS experiences large roll rates and vertical accelerations. However, because of the encounter brevity, the roll angle excursions are still relatively small.

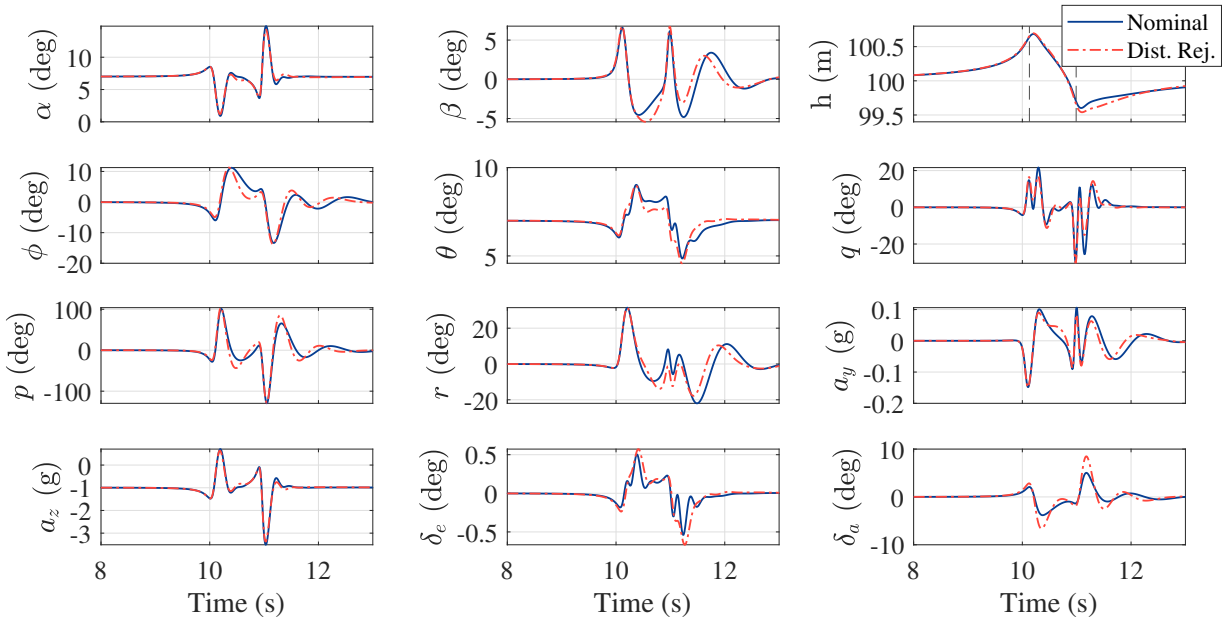

Fig. 11 Case 2: Khawk-55 30° wake vortex encounter (Γ = 20 m^2/s, b = 10 m, r_c = 0.41 m).

Similar trends can be seen for encounters where the UAS crosses perpendicularly behind the generating aircraft, even for wakes of larger sizes, as in Case 3. For perpendicular encounters, the response is almost exclusively in the longitudinal degrees of freedom, shown in Fig. 12. Even with the larger wake generated from a 30-meter-wingspan aircraft, the response is too quick for the controller to alleviate. The control lags slightly behind the response to the wake, and thus the more aggressive controller increases the response severity. The UAS briefly experiences large vertical loads and pitch rates.

Lastly, the opposite phenomenon can be seen for slow, drawn-out encounters like Case 4. In Fig. 13, the UAS was simulated to fly through the wake of the aforementioned small general aviation aircraft. The wake is generated at a 10-degree climb angle, and the UAS crosses the wake at a 15-degree encounter angle. The encounter is slow and drawn-out, and the UAS only crosses through one of the vortex cores. As such, even though the core radius is small, the disturbance rejection controller alleviates the roll response, though the difference is marginal. The roll angle excursion is the largest of any of the four simulated scenarios, and the aileron saturates. This indicates the significant hazard presented by this type of vortex encounter, where the UAS is near the vortex core for a long period of time.

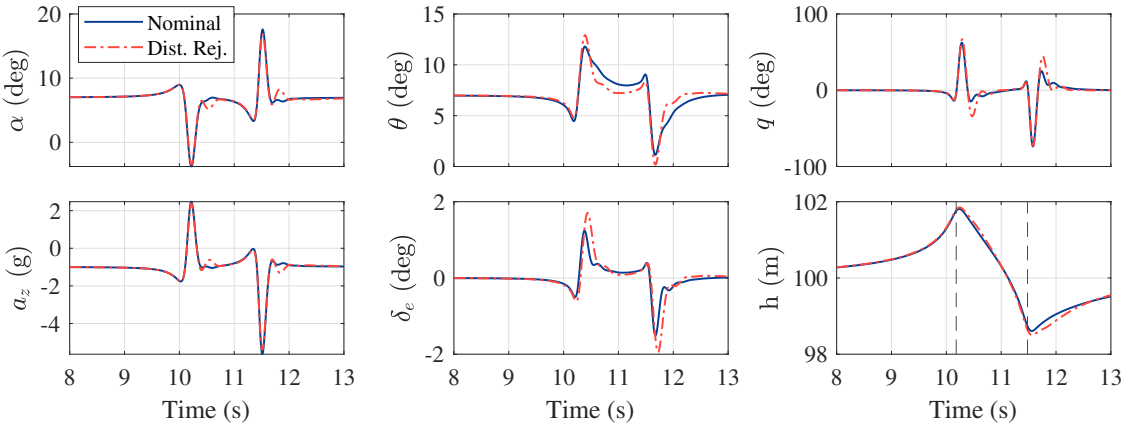

Fig. 12 Case 3: Khawk-55 90° wake vortex encounter (Γ = 100 m^2/s, b = 30 m, r_c = 1.2 m).

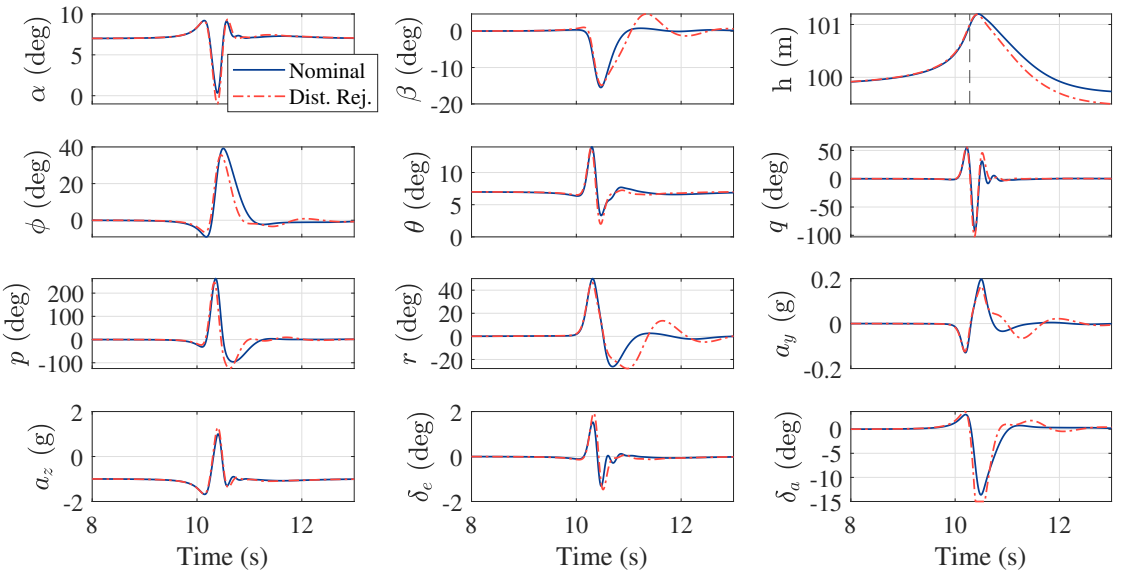

Fig. 13 Case 4: Khawk-55 15° wake vortex encounter (Γ = 20 m^2/s, b = 10 m, r_c = 0.41 m).

VI. Conclusion

A simplified method for modeling and simulating UAS WVEs was proposed, based on the linear wind field approximation. The effect of the wake vortex is approximated as a wind field that is linearly varying in space. The UAS velocities relative to the linear wake field are computed for use with a standard flight dynamics model. This approach allows for rapid computation of many different UAS and WVE scenarios without requiring extra aerodynamic models or explicit geometry definition. Two controllers were designed to evaluate the impact of the inner loop flight control on the WVE. These controllers were based on specifications for nominal conditions and for maximized disturbance rejection. Simulation results showed that the disturbance rejection controller successfully attenuated the UAS WVE response for cases where the encounter was prolonged because of the vortex size or encounter angle. However, for rapid WVEs, such as during flight perpendicular to the wake, both controllers show similar performance, and, if the controller lags behind the response, the more aggressive disturbance rejection controller may increase the severity of the encounter.

In the future, the methods in this paper can be extended to more WVE scenarios and various UAS. By performing large-scale simulation, trends in UAS WVEs could be identified and used to make recommendations for safe UAS operation at airports. These results could be used for wake separation categorization similar to those developed for manned aircraft. Finally, selective experiments are needed to draw conclusions on the accuracy of these methods.

Acknowledgements

This work is supported in part by the University of Kansas School of Engineering Research and Innovation Seed (RISe) Funding and by the Federal Aviation Administration Center of Excellence for Unmanned Aircraft Systems Grant 15-C-UAS-KU-05.

References

[1] Lang, S., Tittsworth, J., Bryant, W., Wilson, P., Lepadatu, C., Delisi, D., Lai, D., and Greene, G., "Progress on an ICAO Wake Turbulence Re-Categorization Effort," *AIAA Atmospheric and Space Environments Conference*, 2010. https://doi.org/10.2514/6.2010-7682.

[2] Cheng, J., Hoff, A., Tittsworth, J., and Gallo, W. A., "The Development of Wake Turbulence Re-Categorization in the United States (Invited)," *8th AIAA Atmospheric and Space Environments Conference*, 2016. https://doi.org/10.2514/6.2016-3434.

[3] Hallock, J. N., Greene, G. C., Tittsworth, J., Strande, P., and Wang, F. Y., "Use of Simple Models to Determine Wake Vortex Categories for New Aircraft (Invited)," *7th AIAA Atmospheric and Space Environments Conference*, 2015. https://doi.org/10.2514/6.2015-3172.

[4] Tatnall, C. R., "A Proposed Methodology for Determining Wake-Vortex Imposed Aircraft Separation Constraints," Master's thesis, George Washington University, 1995.

[5] Pete, K., Smith, S., and Vicroy, D., "Model validation for wake-vortex/aircraft encounters," *Atmospheric Flight Mechanics Conference*, 2000. https://doi.org/10.2514/6.2000-3979.

[6] Vicroy, D. D., "Influence of wind shear on the aerodynamic characteristics of airplanes," Tech. Rep. NASA-TP-2827, 1988.

[7] Reimer, H. M., and Vicroy, D. D., "A Preliminary Study of a Wake Vortex Encounter Hazard Boundary for a B737-100 Airplane," Tech. Rep. NASA-TM-110223, 1996.

[8] Fischenberg, D., "A Method to Validate Wake Vortex Encounter Models from Flight Test Data," *27th International Congress of the Aeronautical Sciences*, 2010.

[9] Anon., "Consolidated Wake Turbulence," Tech. Rep. JO 7110.126B, Federal Aviation Administration, November 2021.

[10] Nguyen, N. T., "A Physics-Based Spatial Wake Interactional Model of Fixed-Wing Aircraft and Rotorcraft for Urban Air Mobility," *AIAA Scitech 2021 Forum*, 2021. https://doi.org/10.2514/6.2021-0881.

[11] Nguyen, N. T., Bartolini, G., Baculi, J. E., Okolo, W., and Xiong, J., "Wake Vortex Interaction of Urban Air Mobility Aircraft," *AIAA SCITECH 2022 Forum*, 2022. https://doi.org/10.2514/6.2022-1031.

[12] Tian, P., He, A., Chao, H., Zheng, Z. C., and Gu, Y., "Wake Encounter Simulation and Flight Validation with UAV Close Formation Flight," *AIAA Guidance, Navigation, and Control Conference*, 2017. https://doi.org/10.2514/6.2017-1910.

[13] He, A., Zheng, Z. C., Chao, H., Tian, P., and Gu, Y., "A Study on Wake Turbulence Encounter during UAV Formation Flight Using Coupled Aerodynamics/Flight Dynamics Simulation (Invited)," *8th AIAA Atmospheric and Space Environments Conference*, 2016. https://doi.org/10.2514/6.2016-3439.

[14] Lin, Z., Matt, J. J., Chao, H., Zheng, Z. C., and Ewing, M., "Wake Vortex Modeling and Simulation for Small Fixed-Wing UAS with Inner Loop Attitude Control," *AIAA 2022 Aviation Forum*, 2022.

[15] Beard, R. W., and McLain, T. W., *Small Unmanned Aircraft: Theory and Practice*, 1st ed., Princeton University Press, Princeton, NJ, 2012.

[16] Flanagan, H. P., Chao, H., and Hagerott, S. G., "Model Based Roll Controller Tuning and Frequency Domain Analysis for a Flying-Wing UAS," *2019 International Conference on Unmanned Aircraft Systems (ICUAS)*, 2019, pp. 721–728. https://doi.org/10.1109/ICUAS.2019.8798212.

[17] Matt, J. J., Hagerott, S. G., Svoboda, B. C., Chao, H., and Flanagan, H. P., "Frequency Domain System Identification of a Small Flying-Wing UAS," *AIAA SCITECH 2022 Forum*, 2022. https://doi.org/10.2514/6.2022-2407.

[18] Etkin, B., "Turbulent Wind and Its Effect on Flight," *Journal of Aircraft*, Vol. 18, No. 5, 1981, pp. 327–345. https://doi.org/10.2514/3.57498.

[19] Hallock, J. N., and Eberle, W. R., "Aircraft Wake Vortices: A State-of-the-Art Review of the United States R&D Program," Tech. Rep. FAA-RD-77-23, U.S. Department of Transportation, February 1977.

[20] Burnham, D., Hallock, J., Tombach, H., Brashears, M., and Barber, M., "Ground-Based Measurements of the Wake Vortex Characteristics of a B-747 Aircraft in Various Configurations," Tech. Rep. FAA-RD-78-146, U.S. Department of Transportation, Dec 1978.

[21] Sarpkaya, T., "New model for vortex decay in the atmosphere," *Journal of Aircraft*, Vol. 37, No. 1, 2000, pp. 53–61. https://doi.org/10.2514/2.2561.

[22] Dogan, A., Venkataramanan, S., and Blake, W., "Modeling of Aerodynamic Coupling Between Aircraft in Close Proximity," *Journal of Aircraft*, Vol. 42, No. 4, 2005, pp. 941–955. https://doi.org/10.2514/1.7579.

[23] Anon., "Flight Control Systems - Design, Installation And Test Of Piloted Aircraft, General Specification For," Tech. Rep. MIL-DTL-9490E, Department of Defense, April 2008.

[24] Anon., "Flying Qualities of Piloted Aircraft," Tech. Rep. MIL-STD-1797B, Department of Defense, February 2006.

[25] Blanken, C. L., Hoh, R. H., and Mitchell, D. G., "Test Guide for ADS-33E-PRF," Tech. Rep. AMR-AF-08-07, US Army RDECOM, July 2008.

[26] Sanders, F. C., Tischler, M., Berger, T., Berrios, M. G., and Gong, A., "System Identification and Multi-Objective Longitudinal Control Law Design for a Small Fixed-Wing UAV," *AIAA Atmospheric Flight Mechanics Conference*, 2019. https://doi.org/10.2514/6.2018-0296.

[27] Matt, J. J., Flanagan, H., and Chao, H., "Evaluation and Analysis of ArduPilot Automatic Tuning Algorithm for the Roll Tracking Controller of a Small UAS," *AIAA Scitech 2021 Forum*, 2021. https://doi.org/10.2514/6.2021-0016.

[28] Berger, T., Ivler, C., Berrios, M., Tischler, M., and Miller, D., "Disturbance Rejection Handling Qualities Criteria for Rotorcraft," *AHS 72nd Annual Forum*, 2016.